Article

Molecular Cell

Structural Visualization of the Formation and Activation of the 50S Ribosomal Subunit during *In Vitro* Reconstitution

Graphical Abstract

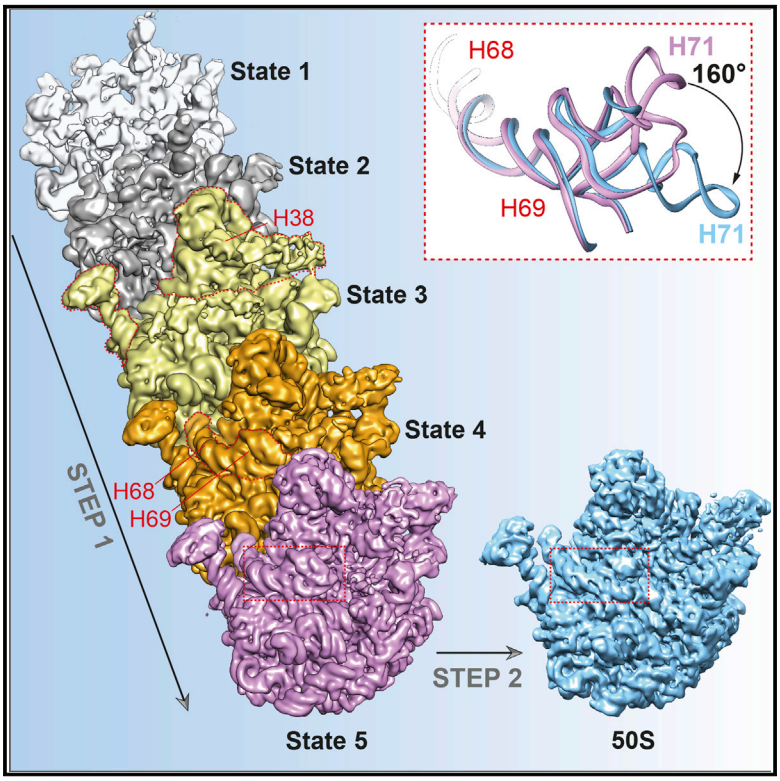

Authors

Rainer Nikolay, Tarek Hilal, Bo Qin, ..., Kathrin Textoris-Taube, Knud H. Nierhaus, Christian M.T. Spahn

Correspondence

christian.spahn@charite.de

In Brief

Nikolay et al. present cryo-EM reconstructions of *in-vitro*-generated large ribosomal subunit precursors, which showcase how successive binding of ribosomal proteins is paralleled by formation and stabilization of rRNA folds. These findings establish a basis for a deeper mechanistic understanding of ribosome assembly and will inspire future *in vivo* approaches.

Highlights

- High-resolution cryo-EM reveals five distinct structural 50S precursor intermediates
- Ribosomal proteins influence RNA folding, thereby acting as built-in assembly helpers
- Appearance of the protuberances defines transition from 41S to 48S precursors
- 50S activation requires reorientation of 23S rRNA H71 and stable formation of H90-93

Nikolay et al., 2018, Molecular Cell *70*, 881–893
June 7, 2018 © 2018 Elsevier Inc.
https://doi.org/10.1016/j.molcel.2018.05.003

CellPress

Molecular Cell
Article

Structural Visualization of the Formation and Activation of the 50S Ribosomal Subunit during *In Vitro* Reconstitution

Rainer Nikolay,[1,5] Tarek Hilal,[1,5] Bo Qin,[1] Thorsten Mielke,[2] Jörg Bürger,[1,2] Justus Loerke,[1] Kathrin Textoris-Taube,[3] Knud H. Nierhaus,[1,4] and Christian M.T. Spahn[1,6,*]
[1]Institut für Medizinische Physik und Biophysik, Charité – Universitätsmedizin Berlin, corporate member of Freie Universität Berlin, Humboldt-Universität zu Berlin, and Berlin Institute of Health, Berlin, Germany
[2]UltraStrukturNetzwerk, Max Planck Institute for Molecular Genetics, Berlin, Germany
[3]Institute of Biochemistry, Shared Facility for Mass Spectrometry, Charité – Universitätsmedizin Berlin, corporate member of Freie Universität Berlin, Humboldt-Universität zu Berlin, and Berlin Institute of Health, Berlin, Germany
[4]Department Vingron, Max Planck Institute for Molecular Genetics, Berlin, Germany
[5]These authors contributed equally
[6]Lead Contact
*Correspondence: christian.spahn@charite.de
https://doi.org/10.1016/j.molcel.2018.05.003

SUMMARY

The assembly of ribosomal subunits is an essential prerequisite for protein biosynthesis in all domains of life. Although biochemical and biophysical approaches have advanced our understanding of ribosome assembly, our mechanistic comprehension of this process is still limited. Here, we perform an *in vitro* reconstitution of the *Escherichia coli* 50S ribosomal subunit. Late reconstitution products were subjected to high-resolution cryo-electron microscopy and multiparticle refinement analysis to reconstruct five distinct precursors of the 50S subunit with 4.3–3.8 Å resolution. These assembly intermediates define a progressive maturation pathway culminating in a late assembly particle, whose structure is more than 96% identical to a mature 50S subunit. Our structures monitor the formation and stabilization of structural elements in a nascent particle in unprecedented detail and identify the maturation of the rRNA-based peptidyl transferase center as the final critical step along the 50S assembly pathway.

INTRODUCTION

Bacterial 70S ribosomes are macromolecular complexes consisting of two distinct subunits, the small 30S and the large 50S. Both subunits are composed of rRNA and ribosomal proteins (r-proteins). The 30S subunit contains a single 16S rRNA and 21 r-proteins, while the 50S subunit is composed of two rRNAs (23S and 5S rRNA) and 33 r-proteins. Ribosomal subunit assembly is an orchestrated multi-step process, involving the production, processing, folding, and modification of rRNAs and r-proteins (Kaczanowska and Rydén-Aulin, 2007). These RNA and protein components undergo a series of highly ordered interactions and binding events, resulting in the formation of functional subunits. *In vivo*, this complex process is steered and regulated by numerous maturation and assembly factors (Kaczanowska and Rydén-Aulin, 2007; Shajani et al., 2011). These groups of factors include RNases, GTPases, ATPases, and different enzymes that chemically modify rRNA and r-proteins (Kaczanowska and Rydén-Aulin, 2007). Their individual contributions are typically investigated by gene deletion experiments. When combined with ribosome profiles, SDS, or western blot analyses, and more recently with quantitative mass spectrometry approaches, such studies provided estimates of assembly defects or identification of r-proteins lacking from immature subunits (Britton, 2009; Jomaa et al., 2014; Li et al., 2013a).

In order to obtain structural information for 50S subunit precursors, assembly factors were similarly depleted and accumulating precursors were visualized at intermediate resolution using cryo-electron microscopy (cryo-EM). For example, deletion of the GTPases *rbgA* (Jomaa et al., 2014; Li et al., 2013a), *yphC*, and *ysxC* (Ni et al., 2016) yielded intermediate-resolution structures of accumulating 50S precursors that lack structural elements, specifically the central protuberance. In the two latter cases, only the core of the 50S subunit was resolved, indicating a more immature state. A recent structural study analyzed alternative assembly pathways yielding incomplete 50S subunits arising upon depletion of an essential r-protein (bL17), demonstrating that 50S assembly is highly dynamic under conditions of r-protein scarcity and becomes rerouted (Davis et al., 2016). However, while these special case scenarios revealed snapshots of 50S precursors accumulating in the absence of an r-protein or assembly factors, the question remains what intermediates are populated under conditions of unperturbed 50S assembly.

In a complementary approach to study ribosomal subunit assembly, pioneering *in vitro* approaches in the bacterial system demonstrated that purified rRNAs and r-proteins self-assemble to fully active ribosomal subunits (Nierhaus and Dohme, 1974;

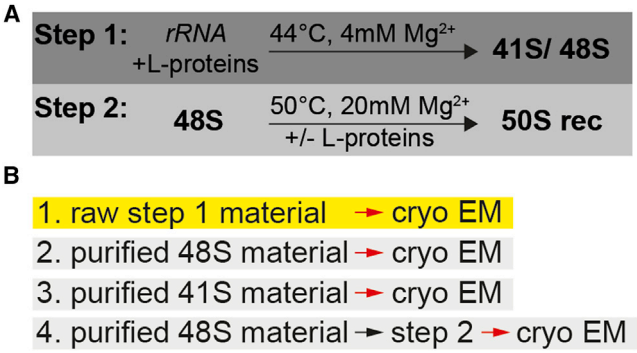

Figure 1. Workflow and Experimental Strategy

(A) Workflow of 50S reconstitution: ribosomal RNA (rRNA) and proteins of the large subunit (L-proteins) were subjected to the step 1 reaction (dark gray), yielding 41S and 48S precursors. Either the non-purified products (raw step 1 material), purified 48S, or purified 41S material was used for further analyses. Purified 48S material was subjected to a step 2 reaction in the presence or absence of L-proteins (±L-proteins) generating reconstituted 50S subunits (50S rec).

(B) Experimental strategy: (1) The step 1 reaction was performed for 30 min, and the non-purified raw material was subjected to cryo-EM analysis. (2) The step 1 reaction was performed. Material corresponding to the 48S peak was purified and analyzed by cryo-EM. (3) The step 1 reaction was performed. Material corresponding to the 41S peak was purified and analyzed by cryo-EM. (4) The step 1 reaction was performed. Material corresponding to the 48S peak was purified, subjected to a step 2 reaction in the presence of L-proteins yielding 50S rec^{+}, which was analyzed by cryo-EM.

See also Figures S1 and S5.

Traub and Nomura, 1968). Despite the fact that in comparison to *in vivo* assembly, *in vitro* reconstitution requires prolonged time, higher salt concentrations, and elevated temperatures, this remarkable observation indicates that the blueprint of assembly is inherent in the ribosomal components themselves. Thus, the *in vitro* reconstitution systems provides a unique minimal system for studying intrinsic assembly pathways in the absence of pharmacologic or genetic manipulations (Dohme and Nierhaus, 1976b; Nierhaus and Dohme, 1974; Traub and Nomura, 1968), limiting indirect effects and facilitating analysis. Biochemical studies in the *in vitro* system revealed that rRNA sequentially recruits r-proteins in a hierarchical fashion. Order of addition and single-omission experiments with r-proteins elaborated assembly maps of this hierarchical recruitment mechanism (Herold and Nierhaus, 1987; Mizushima and Nomura, 1970), reflecting both the order of r-protein incorporation and the interdependency of individual r-proteins within this process. Importantly, precursor particles of the large subunit obtained from both *in vitro* and *in vivo* approaches are similar in size and composition, with sedimentation S-values of ~33S, ~41S, and ~48S, respectively (Shajani et al., 2011).

While the *in vitro* reconstitution approach has been used to reveal biochemical landmarks of subunit assembly under defined conditions (Nierhaus, 1991), a mechanistic understanding of bacterial ribosome assembly is lacking structural data to disentangle distinct precursors along their intrinsic assembly pathway. In order to reveal the intrinsic molecular principles of 50S assembly, we performed *in vitro* reconstitution studies with purified ribosomal RNA and protein components under defined and scalable conditions, and employed high-resolution cryo-EM to yield five structures of distinct 50S assembly intermediates at resolutions of 4.3–3.8 Å. Our analysis provides a structural framework for the 50S assembly pathway *in vitro*, revealing that the rate-limiting maturation events mainly involve the three 50S protuberances and the peptidyl transferase center (PTC). Interestingly, structural reorganizations appear to coincide with the incorporation of the late assembly proteins bL33, bL35, and uL16. The most mature precursor particle resembles a native 50S subunit but possesses disordered elements of rRNA within the PTC region corresponding to helices H71 and H90–H93, whose native folding requires a heat activation step at elevated Mg^{2+} concentration. Thus, stable formation and native positioning of RNA helices in the PTC is the final critical step for generating catalytically active 50S subunits from inactive 48S precursor particles.

RESULTS

Generation of 50S Precursors by Total *In Vitro* Reconstitution

In order to prepare late precursors of the ribosomal 50S subunit suited for high-resolution cryo-EM studies, we revisited the *in vitro* reconstitution approach. *In vitro* reconstitution of large ribosomal subunits from purified rRNAs and total r-proteins requires a two-step protocol (Nierhaus and Dohme, 1974). At rate-limiting steps during assembly, transient precursor particles arise that are on-pathway intermediates with a partial r-protein complement. During *in vitro* assembly (Figure S1A), the most immature 33S particle occurs within seconds, while after 30 min, 41S and 48S particles prevail (Dohme and Nierhaus, 1976b; Sieber and Nierhaus, 1978). The ultimate product of step 1 is the 48S particle that is thought to contain all r-proteins but is inactive in translation unless subjected to step 2, in which it is converted into a mature 50S subunit under the influence of high Mg^{2+} concentration (20 mM) and thermal energy (50°C) (Dohme and Nierhaus, 1976b; Nierhaus, 1991). To verify that the particles obtained during *in vitro* reconstitution of 50S subunits in our experimental setup represent genuine 50S precursors and not dead-end particles, we performed a time course of the first and second reaction. Indeed, the precursors were transformed into a homogeneous final population (Figures S1B–S1M).

Structural Analysis of *In Vitro* Reconstituted Ribosomal Particles

To prepare late 50S precursors for structural studies, we performed step 1 of the reconstitution reaction (Figure 1A), which delivers 41S and 48S reconstitution intermediates but no mature 50S subunits (Nierhaus, 1991). As expected, the intermediates obtained in step 1 were inactive in translation and required a second incubation (step 2) with high temperature and magnesium concentration to be converted into active, *in vitro* reconstituted 50S particles (50S rec). The activity assay showed that the step 2 reaction resulted in ~70% activity (Figure S1N) compared with native 50S subunits (50S) and is within the activity range of 60%–100% that is commonly achieved by reconstitution procedures (Dohme and Nierhaus, 1976b). We subjected the

non-purified step 1 material to cryo-EM analysis (Figure 1B). The refinement revealed five different reconstructions corresponding to precursors of the 50S subunit at different maturation stages as indicated by differences in protein density, amount of natively folded rRNA, and diverging conformation (Figure S2A). The similarity to the mature 50S subunit increases sequentially from the least (state 1) to most mature (state 5) particle.

In order to limit heterogeneity of the specimen and focus on late assembly intermediates, a preparative step 1 reaction was performed, and then these step 1 reaction products were further subjected to sucrose density gradient centrifugation and subsequent fractionation (Figure S1O). In order to demonstrate that this purification step did not impair the integrity of the 50S precursors (e.g., by shearing off r-proteins), fractions containing the 48S peak were pooled and aliquots were subjected to (1) analytical sucrose density centrifugation (Figure S1O, insert), (2) the second step activation reaction, (3) cryo-EM analyses, or (4) activity assays (Figure S1P). The translation assay revealed that the material from the 48S peak reached ~80% activity when converted to 50S rec by the step 2 reaction compared with native 50S. Interestingly, 48S material subjected to the second incubation step in the presence or absence of large subunit proteins (L-proteins) achieved comparable activity, indicating that 48S particles contain all L-proteins relevant for activity. To determine the protein complement, 48S material was subjected to quantitative mass spectrometry analysis. The presence of uL1, bL7/12, uL10, and uL11, which escape detection by cryo-EM due to high structural flexibility, was confirmed (Figure S3A). However, bL31 and bL36 were present at sub-stoichiometric levels. bL31 is a loosely attached r-protein with a long flexible alpha helix that extends to and interacts with the 30S subunit, and it has been shown to easily dissociate from 50S subunits (Eistetter et al., 1999). Crystal structures of 70S ribosomes have been solved lacking bL36 (Selmer et al., 2006), indicating that the protein can be lost even from mature ribosomes, depending on buffer conditions.

Multi-particle cryo-EM analysis of purified material derived from the 48S peak resulted in four distinct cryo-EM maps at near-atomic resolutions between 4.9 Å and 3.8 Å (Figure S2B). The majority of the reconstituted states correspond to late assembly intermediates already identified in the non-purified step 1 material. The reconstruction for the earliest intermediate appears to be a mixture of state 1 and state 2 that could not be sorted further due to the low particle image number. Because states 1 and 2 were already resolved from the non-purified step 1 material (Figures 2A and 2B), we used these along with the cryo-EM reconstructions for states 3–5 (Figures 2C–2E) for modeling. Local resolution estimates indicate that the core region of the respective particles is well defined, while peripheral elements are less resolved due to flexibility or ongoing maturation (Figure S3B).

Why is there such conformational diversity in purified 48S material? We noticed that the 48S peak is slightly asymmetric, with a shoulder on the left (lighter) side (Figure S1O, insert), and wondered whether 41S and 48S material is cross-contaminated due to close proximity of the peaks. To test this hypothesis, we isolated material corresponding to the 41S peak (Figure S1Q) and analyzed it by analytical sucrose density centrifugation and cryo-EM. Of note, the purified 41S material shows a distinct shoulder on the right (heavier) side (Figure S1Q, insert), which presumably is due to contamination with 48S material. Concordantly, initial reconstruction and sorting revealed a conformational diversity within the 41S material as well (Figure S2C). However, the distribution of the states is opposite that of the 48S material (Figure S4). In the 41S material, the most immature states 1 and 2 correspond to a major fraction of 64% of the particle images but represent only 8% of the particles in the 48S material. Conversely, in the 48S material, the more mature states 3–5 are enriched to 81% compared with 36% in the 41S material. Thus, we conclude that states 1 and 2 represent 41S, and states 3–5 represent 48S reconstitution intermediates. A major difference is the absence (41S particles) or presence (48S particles), respectively, of the central protuberance (CP) (Figure 2), likely explaining the different sedimentation behavior.

In order to show directly that the precursor particles obtained from step 1 incubation are not dead-end particles, we subjected an aliquot of purified 48S peak material to step 2 incubation followed by cryo-EM analysis. In line with 80% activity of the resulting 50S rec$^+$, and a homogeneous peak in the analytical sucrose gradient profile (Figure S5), structural analysis revealed a fully mature 50S particle (Figures 2F and S5E). Together, these independent reconstitution experiments confirm the authenticity of the individual states derived from raw and pre-purified step 1 material as genuine 50S precursors of the total *in vitro* reconstitution pathway (Figure S4). Because similarity to the mature 50S subunit increases sequentially from the least (state 1) to most mature (state 5) particle, we concluded that these five reconstructions of 50S precursors together with the reconstruction of the mature 50S rec$^+$ particle define a sequential maturation pathway during *in vitro* 50S assembly (Figures 2A–2F).

State 1: The Core Is Structured and Density for Protuberances Is Absent

The earliest conformer in our reconstruction (state 1) is lacking density for the three protuberances of the 50S subunit (CP; L1 protuberance; and stalk base [sb]), whereas the core of the particle is already well defined (Figures 2A, 3A, and 4A) and contains fully folded 23S rRNA of domains I, III, and VI (Figure 5). Remarkably, even in this relatively early state, the protein-rich region surrounding the polypeptide tunnel exit and surrounding solvent surface of the particle are widely mature and hardly distinguishable from a 50S subunit (Figure 2A, back view). The map exhibits clear density for 16 r-proteins, including all five early essential assembly L-proteins (uL4, uL13, bL20, uL22, and uL24), which are necessary and sufficient to initiate *in vitro* assembly (Spillmann et al., 1977) (Figure 2A; Table S1). Notably, state 1 resembles a large subunit precursor structure recently resolved at intermediate resolution from an *in vivo* preparation (Ni et al., 2016), reinforcing the validity of our *in vitro* approach.

Outside of the well-defined 50S core, some fragmented density indicates heterogeneity due to dynamic, not yet stably incorporated proteins or fully folded rRNA elements. For uL3 and uL15, only partial density is present, corresponding to the N and C termini, while the extended intermediate segments are

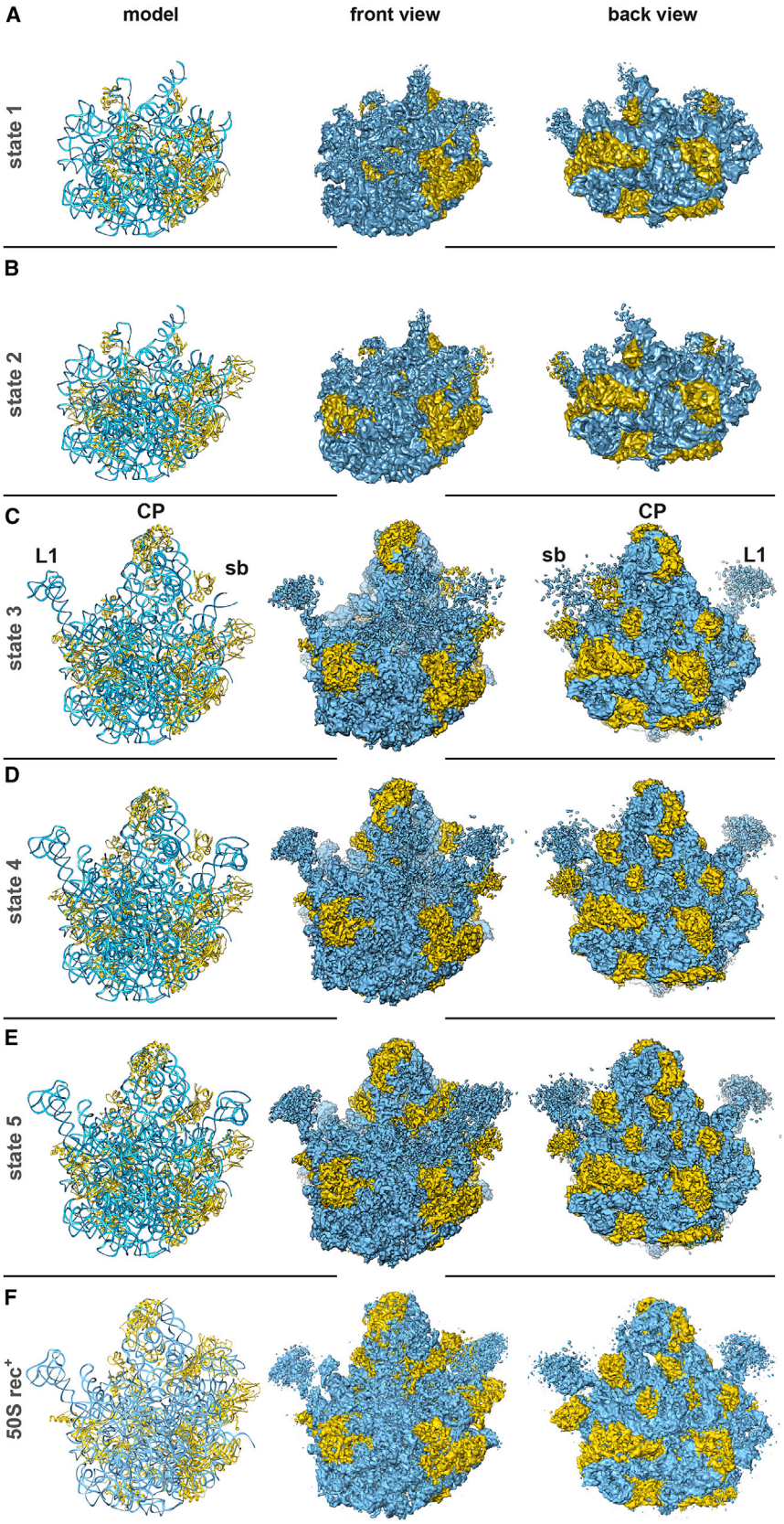

Figure 2. Structural Representation of Five Distinct 50S Subunit Precursor States

(A–F) Atomic models (first column), front views (second column), and back views (third column) of electron density maps of state 1 (A), state 2 (B), state 3 (C), state 4 (D), state 5 (E) and 50S rec^{+} (F) (pooled 48S material subjected to step 2 reaction in the presence of TP50). L-proteins are colored in gold and r-RNA in blue. CP, central protuberance; L1, L1stalk; sb, stalk base. See also Figures S2–S6 and Tables S1 and S2.

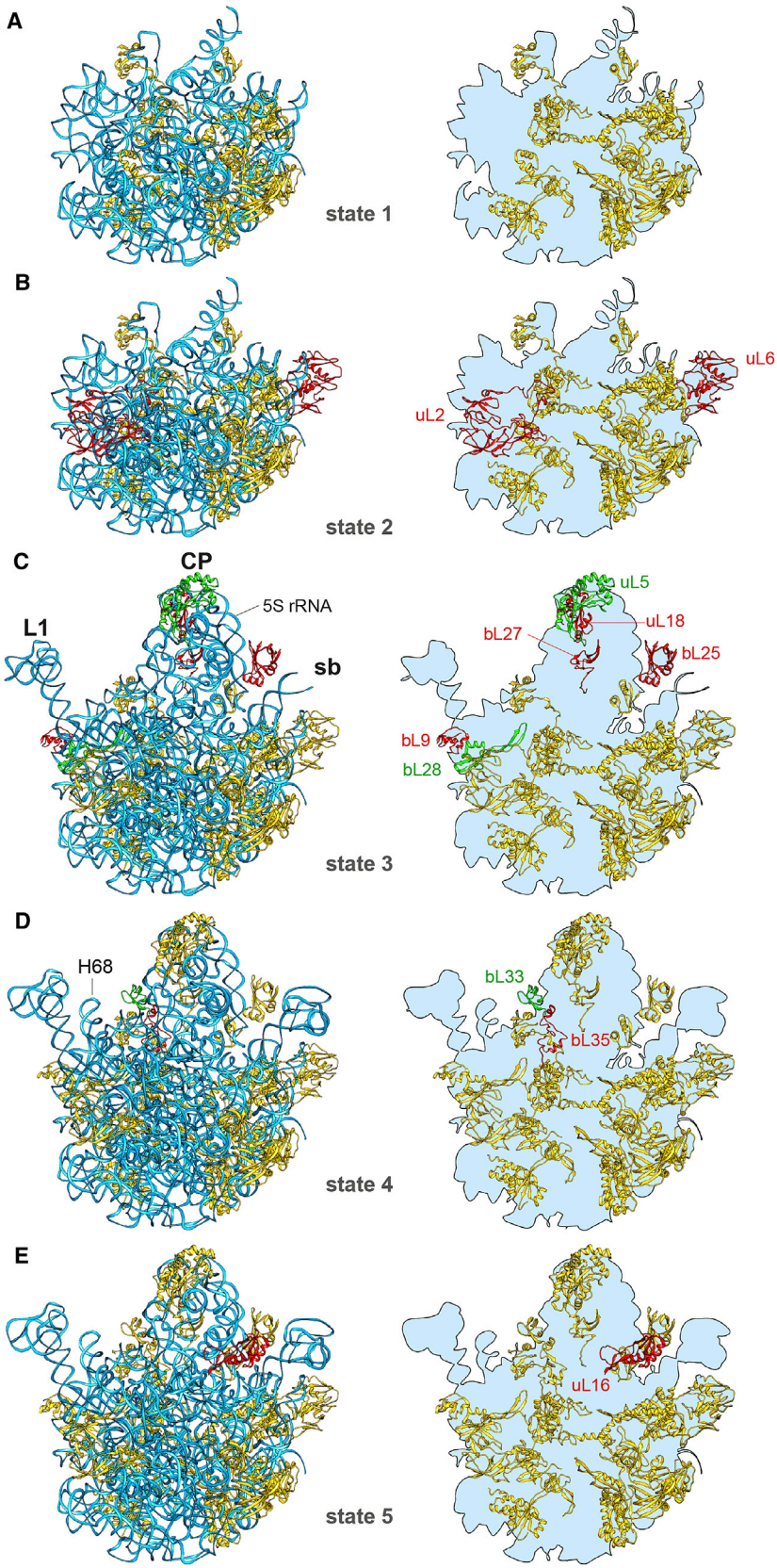

Figure 3. Structural Conformation and Protein Composition of States 1–5

(A–E) States 1–5. Left column: atomic models showing 23S rRNA and 5S rRNA in blue and L-proteins for which electron density is found already in state 1 (A) in gold. R-proteins appearing first in states 2 (B), 3 (C), 4 (D), or 5 (E) are highlighted in green or red. Right column: corresponding representations with the silhouettes of the particles given as blue area and proteins colored analogous to the left column. CP, central protuberance; L1, L1stalk; sb, stalk base. See also Figure S3.

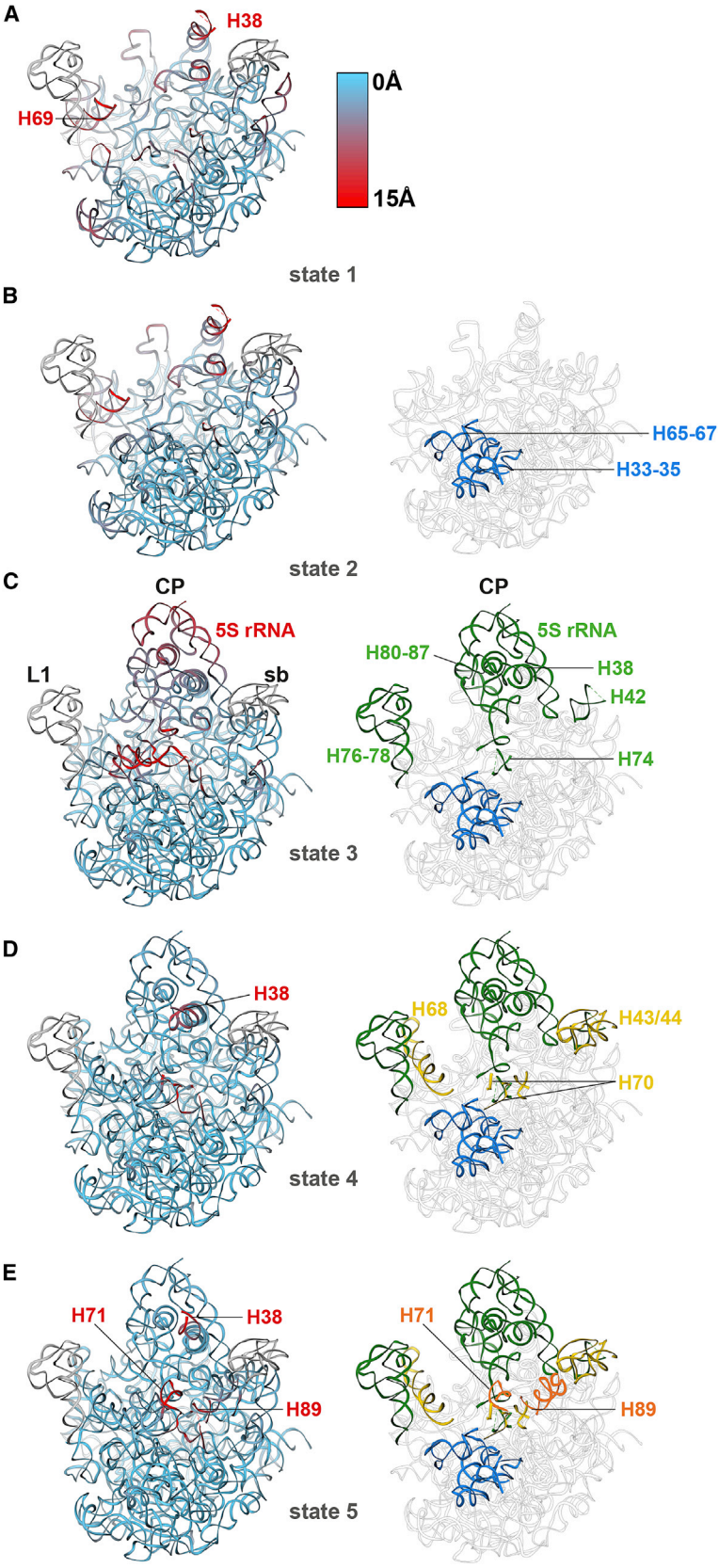

Figure 4. Conformational Dynamics of rRNA in States 1–5

(A–E) States 1–5. Left column: atomic models of the 23S and 5S rRNA of states 1–5. The color code indicates the distance of RNA positions within the models of the individual states, relative to the corresponding positions within the mature 50S subunit (blue 0, red 15A) (A). The color code has not been applied to the L1 stalk and parts of the stalk base, since both elements are intrinsically flexible. Right column: based on a model of the mature state of the *E. coli* large-subunit rRNA (PDB: 3R8S), RNA elements, which are resolved for the first time in state 2 (B), 3 (C), 4 (D), or 5 (E), are colored in blue, green, yellow, or orange, respectively. Some elements show pronounced flexibility; H74 relocates 10–20 Å toward the A-site (C), and helix H71 adopts a non-native position blocking access to the PTC (E).

CP, central protuberance; L1, L1stalk; sb, stalk base.

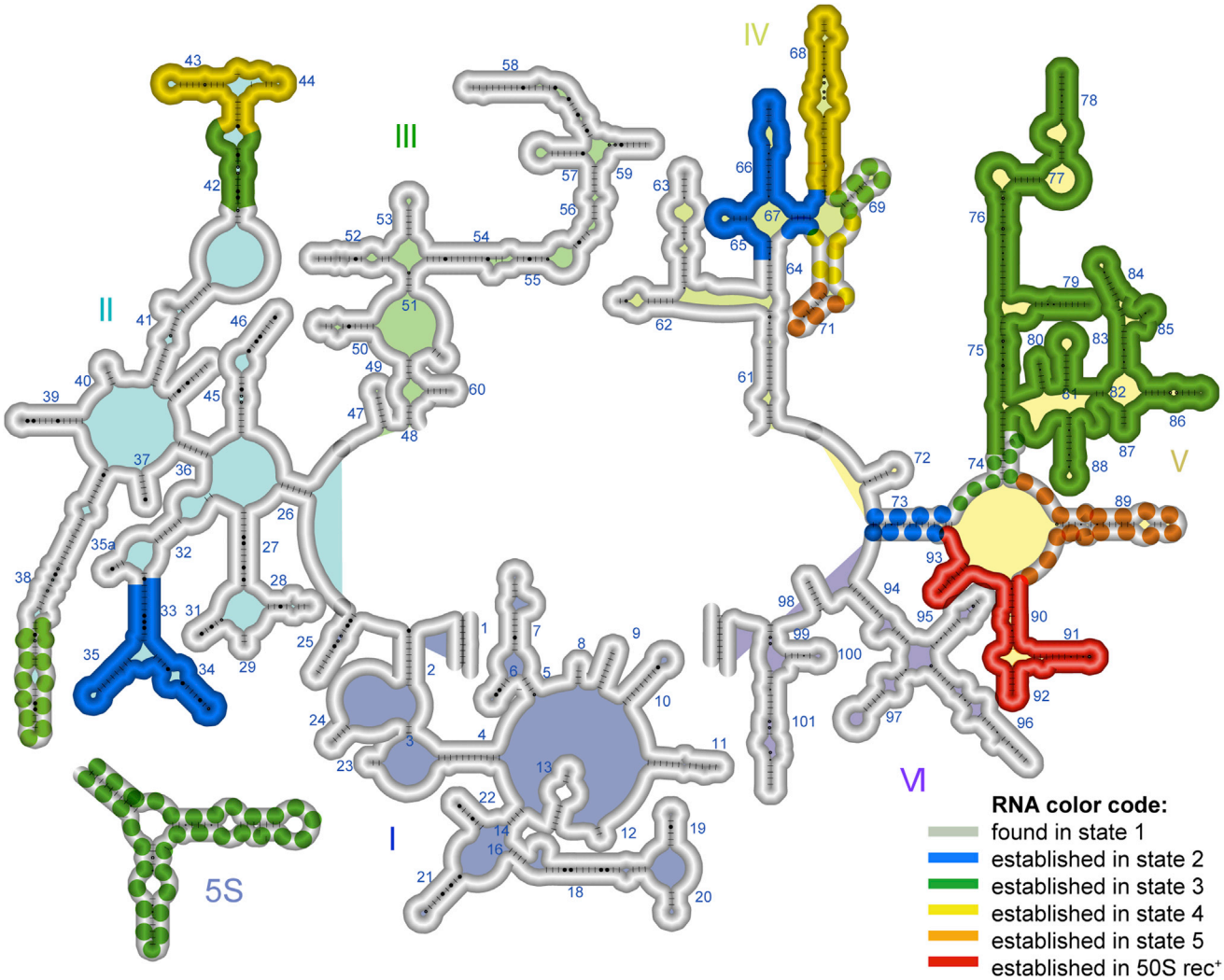

Figure 5. Sequence of rRNA Folding

Secondary structure diagram of 23S and 5S rRNA. Domains I–VI of the 23S rRNA are labeled and filled with corresponding colors. Segments of 23S and 5S rRNA are color-coded depending on the state in which their density was detectable first. Regions for which density was first found in state 1, 2, 3, 4, or 5 are colored gray, blue, green, yellow, or orange, respectively. Dotted color denotes regions for which density appeared at the indicated state but was followed by structural rearrangements in later states. Regions for which density is lacking also in state 5 are shown in red. Adopted from *E. coli* 23S rRNA secondary structure, which is available from the web page of the Noller laboratory (http://rna.ucsc.edu/rnacenter/images/figs/ecoli_23s.jpg). See also Figure S7.

unresolved. Moreover, further sorting of the state 1 cryo-EM particle images from the 41S peak material resulted in the substates 1A and 1B (Figure S2C). These do not exhibit major distinctions in the already stable assembled 50S core but show differences that appear to be caused by fluctuations in dynamic RNA elements such as helices H38 and H34–H35.

State 2: The Core Is Completed

State 2 provides strongly fragmented density for uL6, which seems to be highly flexible, and almost complete density for uL2. While uL6 is positioned underneath the sb, for which density is still lacking, binding of uL2 contributes to the completion of the core region (Figures 3B and 4B). This is supported by interactions between the extended C-terminal region of uL2 and helices H33 to H35, which adopt a stable conformation. Further, density for H66 appears, which engages with uL2. The structural changes accompanying the appearance of uL2 provide the basis for the assembly of further building blocks that initiate CP formation.

State 3: Density for the Protuberances Appears

State 3 contains density for the L1 protuberance and most parts of the CP including the tip of the A-site finger (H38) (Figure 3C). Accordingly, 50S assembly proceeds from state 2 to state 3 with the incorporation of a set of five r-proteins and the docking of a preformed complex consisting of 5S rRNA, uL5, and uL18 (Herold and Nierhaus, 1987) (Table S1). Furthermore, the upper part of domain V with helices H76–H78 (L1 protuberance) and helices H80–H87 (CP) becomes folded into the mature state

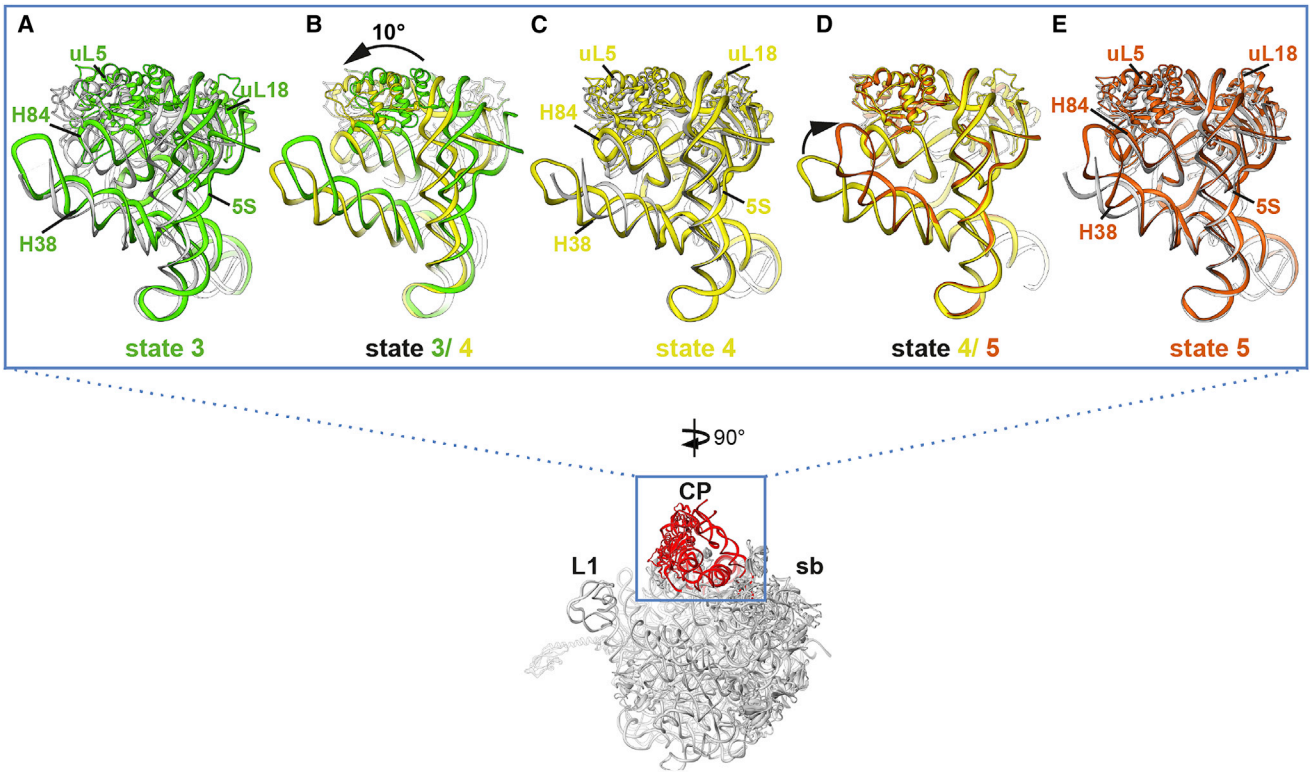

Figure 6. Structural Flexibility within the Central Protuberance

Shown are sections of the of the *E. coli* 50S model (PDB: 3R8S) containing parts of the CP as indicated in red and surrounded by a blue square. Magnified are 5S rRNA (5S) helices H38 and H84 and the CP binding proteins uL5 and uL18.

(A) Superimposition of the 50S model (gray) and the corresponding region of state 3 (green).

(B) Superimposition of states 3 and 4 indicating a rotation of the CP as a rigid body movement by 10°C.

(C) Superimposition of the 50S model (gray) and the corresponding region of state 4 (yellow).

(D) Superimposition of states 4 and 5 indicating a relocation of H38. The tip of H38 is undergoing a movement and translocates 16 Å toward uL5, forming an interaction not present in state 4.

(E) Superimposition of the 50S model (gray) and the corresponding region of state 5 (orange).

(Figures 4C and 5). The incorporation of bL28 and bL9, which are positioned underneath the L1 stalk, could support its manifestation. In addition, the complete A-site finger (H38) as part of the CP has formed but awaits final positioning. Density for only a few r-proteins is lacking (uL16, bL33, bL35, and bL36), which all contribute to the architecture of the CP, rendering it an obvious construction site in late assembly.

State 4: H68 Forms and the CP Moves upon bL33 and bL35 Incorporation

The maturation of the CP concludes with the transition from state 3 to state 4. The underlying molecular events are the stable incorporation of bL33 and bL35 (Figure 3D) and a rotation of the CP by ~10° (measured at the 5S rRNA) (Figures 6A–6C). Interestingly, cryo-EM structures of immature large subunits isolated both from bacteria and yeast (Jomaa et al., 2014; Leidig et al., 2014; Wu et al., 2016) exhibit a high structural flexibility associated with 5S rRNA and the entire CP region, indicating that its maturation *in vivo* involves pronounced structural rearrangements as well. The rotation we observe goes along with the formation of 23S rRNA helices H43, H44, H68, and H70, while H69 changes conformation (Figure 4D). These processes mostly affect domain IV forming part of the rim of the PTC cleft. The binding sites of bL33 and bL35 are close to helices H83–H87 within the CP region. Thus, it is conceivable that stable integration of bL33 and bL35 could influence the positioning of the whole CP. Likewise, helices H68 and H69 are in close proximity to the bL33 and bL35 binding sites and could be stabilized by the presence of these two proteins (Figures 3D and 4D).

State 5: uL16 Incorporation Triggers A-Site Finger Rearrangement and Formation of H89

The changes from state 4 to state 5 are less structurally pronounced, but not less functionally important, appearing to proceed with the incorporation of the late assembly protein uL16 (Chen and Williamson, 2013; Herold and Nierhaus, 1987) to facilitate conformational changes in two 23S rRNA helices. Since H89, which is an integral part of the PTC (Burakovsky et al., 2011), and rearrangement of H38 are only resolved in state 5, these are likely to be a direct consequence of uL16 incorporation (Figures 3E, 4E, 6D, and 6E). State 5 contains the full protein complement of a 48S particle (Figure S3A) and has adopted an

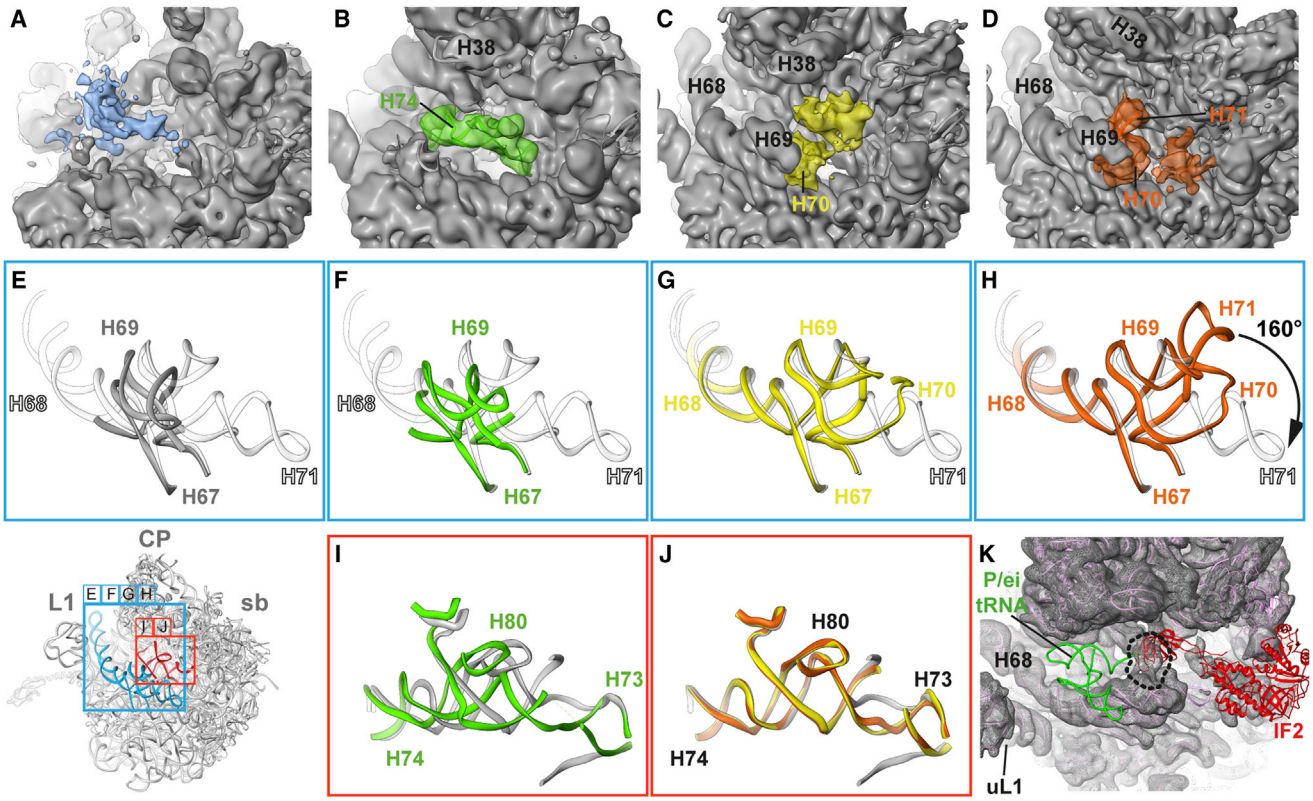

Figure 7. Alternative Structures of the 23S rRNA within the PTC

(A–D) Density maps of states 2–5 are given as gray surface. The dynamic regions within the PTC are indicated by transparent surface representations in blue for state 2 (A), green for state 3 (B), yellow for state 4 (C), and orange for state 5 (D), according to the general color code.

(E–H) *E. coli* 50S model (PDB: 3R8S; Dunkle et al., 2011) for helices H67–H71 is given in light gray, models for helices H67–H71 forming, or changing conformation in state 2 (E), 3 (F), 4 (G), or 5 (H) are shown in gray, green, yellow, or orange, respectively.

(H) The tip of helix 71 rotates ~160° and moves ~59 Å, determined at A1952.

(I and J) Changing positions of helices H73, H74, and H80 in state 3 (green) (I), state 4 (yellow), and state 5 (orange) (J).

(K) Close up of the PTC region of state 4 with IF2-aa-tRNA-fMet (PDB: 3JCJ) superimposed into the model. The factor clashes with the bridge like rRNA formation crossing the PTC. IF2, initiation factor 2; P/ei tRNA, initiator fMet-tRNA$_i^{Met}$.

See also Figure S5.

overall folding similar to mature 50S subunits. This raises important questions: why are 48S particles not active in protein synthesis, and why do they require a heat activation step at elevated Mg^{2+} concentration?

The PTC Remains Immature throughout the Maturation from State 1 to 5

Comparison of the structures of states 1–5 with that of a native 50S particle (Figures 4 and 7A–7H) shows that the most intriguing deviation is the disordered status of the PTC and a high conformational flexibility of parts contributing to inter-subunit bridges. States 2 and 3 exhibit non-native density within the PTC, which seems to be the result of alternative transient RNA formations, incorporating at least H74 (Figure 7I). In state 4, the transient RNA formation has been reordered to involve H70 and H74 repositioning (Figures 7C, 7G, and 7J). Ultimately, density for helix H71 in state 5 appears at a non-native position, where it both interacts with the apical loop of H69 and forms an RNA bridge involving helices H80/81, thereby crossing the region above the PTC (Figures 7D and 7H). This sterically blocks access of an aminoacyl-fMet-tRNA-IF2 initiation complex (Sprink et al., 2016) (Figure 7K), for example, and provides a structural explanation for why 48S particles are excluded from immature translation. In addition, the lower part of domain V including H90–H93 has yet to be formed (Figure 5). This essential region contains most of the nucleotides important for peptide-bond formation and peptide release, such as U2506, U2585, and A2602 (Youngman et al., 2004).

Because all precursors exhibit a non-native RNA meshwork within the PTC region that differs from state 2 to state 5 (Figures 7A–7D) and involves H70, H71, H74, and presumably H90–H93, we propose that proper folding of this important region of 23S rRNA constitutes a critical barrier during the total 50S *in vitro* reconstitution. Native folding of helices H90–H93 appears to be precluded under the conditions of step 1 of the total 50S *in vitro* reconstitution protocol (Figure 1A). Interestingly, the dramatic repositioning of H71 by ~160° that distinguishes state 5 from mature or reconstituted 50S subunits appears to be the critical switch that stabilizes H90–H93 (Figures S5F and S5G). Based on the sequential structural rearrangements in the course

of 50S assembly, we conclude that a substantial reorientation of H71 mediates proper folding of helices H90–H93 and is the final rate-limiting maturation step of 50S *in vitro* assembly that provides functional activity.

DISCUSSION

A Structurally Defined Assembly Pathway for the Total *In Vitro* 50S Reconstitution

The five structures presented here represent a series of successive 50S subunit intermediate assembly states. Together with the structure of the native 50S subunit, or the presented structure of the 50S rec^{+} particle after combined step 1 and step 2 incubations of the total *in vitro* reconstitution protocol as the end point, these structures define a sequential and progressive assembly pathway. They provide unprecedented insight into the mechanism of 50S assembly when solely driven by the physicochemical properties of the rRNAs and the r-proteins. In contrast to *in vivo* assembly inside the cell, rRNA folding and protein incorporation are disentangled from rRNA transcription and modification. Furthermore, *in vitro* reconstitution occurs in the absence of assembly factors. This, on the one hand, leads to significantly prolonged reaction times for *in vitro* 50S assembly, but on the other hand, it allows for structural characterization of assembly intermediates of an unperturbed pathway. Importantly, however, the *in vivo* and the *in vitro* assembly pathways appear highly related (Shajani et al., 2011), implying that the coupling of rRNA synthesis/modification with assembly or the presence of assembly factors do not fundamentally change the blueprint of assembly intrinsic to the ribosomal components.

The two early intermediates of our reconstruction (state 1 and, more clearly, state 2) show an already defined 50S core but lack the three protuberances and the PTC region. The structure of the core particle is essentially indistinguishable from the structure of the corresponding region in the mature 50S subunit. Therefore, the assembly of the 50S core from 23S rRNA domains I, III, and VI and 18 r-proteins can occur independent of the assembly of the protuberances, whereas the assembly of the protuberances and the PTC seems to be dependent on the formation of the 50S core. Comparison of the states derived from 41S material with those derived from 48S material suggests that the stably formed core in states 1 and 2 is a feature of the 41S particle, while appearance of the protuberances in states 3–5 defines the 48S particle.

50S Assembly under Conditions of R-Protein Scarcity

A recent study by Davis et al. (2016) investigated 50S assembly upon depletion of the essential r-protein bL17. The absence of bL17 also prevents bL32, whose assembly is known to be bL17 dependent (Herold and Nierhaus, 1987), from integrating into the large subunit. Interestingly, the bL17-bL32 complex is situated at a strategically significant position in the core of the large subunit. First, this prominent region is located close to the seam of the 23S rRNA, where 5′and 3′ ends meet. Furthermore, it is surrounded by the two early essential proteins bL20 and uL22 and five 23S rRNA domain interfaces (Figures S6A and S6B). These interfaces are rRNA helices connecting domains I and VI (H1), I and II (H2), III and IV (H47/H48 and H61), IV and V (H72 and H73), and V and VI (H73). In addition, helices 96, 99, 100, and 101 of domain VI are in close proximity to bL17 and bL32. Accordingly, the absence of the two proteins renders the core of the subunit unstable (Figures S6C and S6D), thereby provoking the accumulation of particles exhibiting diverse structural deficits. Based on their structural and proteomics approaches, Davis et al. (2016) conclude that 50S assembly in absence of bL17 is rerouted. Accordingly, they arrange the 13 precursor structures that their refinement yields in a flow scheme, with three parallel routes that ultimately merge, to form the most mature but still inactive particle, lacking structural and functional important proteins (bL17, bL32, bL33, and bL35). While our analysis provides insights into a sequential pathway for *in vitro* reconstitution, it has been shown that alternative assembly pathways also exist in this system. For example, reconstitution of 50S subunits using TP50 derived from a mutant strain lacking uL15 and uL30 requires a prolonged step 2 incubation but ultimately generates fully active subunits (Franceschi and Nierhaus, 1990). Similarly, inactive 47S particles reconstituted in the absence of 5S RNA gain full activity upon subsequent addition and integration of 5S RNA (Dohme and Nierhaus, 1976a).

Comparison of Davis et al.'s maturation scheme with our findings reveals similarities and important differences. Our assembly scheme is in general agreement with their main route; however, with substantial differences, as follows. Our earliest state 1 already contains density for bL17 and partial density for bL32, indicating their importance for formation of a stable core. We also observe maturation via distinct building blocks, such as the CP, L1 stalk, stalk base, and the H68/69 ensemble. However, rerouting of assembly in the absence of bL17 involves incorporation of late assembly proteins bL36 and uL16 and maturation of the PTC prior to integration of bL17, bL32, bL33, and bL35 (Davis et al., 2016). This observation is indeed different from both *in vitro* and *in vivo* assembly maps of unperturbed assembly (Chen and Williamson, 2013; Herold and Nierhaus, 1987), while our reconstruction of 50S assembly is in overall agreement with these assembly maps.

Protein Assembly Maps

When comparing the structural evolution of our five states with 50S assembly maps that describe the spatiotemporal association behavior and interdependencies of r-proteins both *in vivo* and *in vitro* (Chen and Williamson, 2013; Herold and Nierhaus, 1987), a number of interesting observations can be made. While r-proteins found to be present in the first state are generally located in the upper left half of the maps, r-proteins appearing from state 2 to state 5 are preferentially found in the lower right half (Figures S7A and S7B). This indicates that at least states 3–5 are late precursors, incorporating late assembly r-proteins in agreement with the assembly maps. Most of the r-proteins appearing in states 3-5 cluster around uL15, which is more obvious in the *in vitro* derived map. The r-protein uL15 is critical for initiating CP formation (Röhl and Nierhaus, 1982), and functionally interacts with uL5 and uL18 that appear concomitantly with 5S rRNA in state 3 (Herold and Nierhaus, 1987). The proteins bL25, bL27, and bL28 that appear in state 3 also depend on uL15. The only state 3 r-protein with no link to uL15 is uL9. Together with bL28, uL9 supports L1 stalk formation, an important hallmark of state 3.

From the state 4 r-proteins, only bL33 was considered in the assembly maps and reported to interact functionally with uL15 and bL28. Due to its low molecular weight of 7.3 kDa, bL35 escaped the detection by classical 2D gel electrophoresis. Nevertheless, previous crystal structures (Dunkle et al., 2011) and our analysis indicate that bL33 and bL35 are situated in proximity to each other, and their presence mediates a movement within the CP region of ~10° (Figure 6B).

The only protein appearing in state 5 is uL16. In fact, many perturbations of 50S assembly, such as pharmacological agents like chloramphenicol, erythromycin, or neomycin (Siibak et al., 2009; Sykes et al., 2010), depletions of assembly factors (Shajani et al., 2011), or truncation of the sarcin-ricin loop (Lancaster et al., 2008) lead to precursors containing reduced levels of late assembly r-proteins and consistently lack uL16. Our findings confirm that uL16 assembles late and suggest that there is a defined order in late 50S assembly that concludes with the incorporation of uL16. Noteworthy, density for the late associating protein bL36 is lacking. Similar to bL35, bL36 also escaped classical assembly mapping experiments due to a low molecular weight. While not essential, incorporation of bL36 was suggested to be an important event in late 50S assembly (Arai et al., 2015). However, quantitative mass spectrometry analysis of purified 48S material revealed 50S-like levels of all r-proteins except bL31 and bL36, whose levels are clearly sub-stoichiometric in the 48S (Figure S3A), despite being stoichiometric in TP50.

rRNA Assembly Map and Protein-Induced Remodeling of rRNA Structures

The structural evolution of our five states also provides detailed insight into the folding of 23S rRNA and defines a sequential order for the mature incorporation of various domains and subdomains of 23S rRNA (Figure 5). In this context, the role of the r-proteins during assembly appears to follow a common principle. Starting from a particle with defined core and extensive unstructured regions (Figures 3A and 4A), the binding of further r-proteins such as bL28, bL9, and uL16 stabilizes rRNA regions locally (Figures 3C, 3E, 4C, and 4E) and binding of bL33 and bL35 more distantly (Figures 3D and 4D) by lowering their degree of conformational freedom. Such a protein-induced remodeling of RNA structures has been suggested for some ribonucleoprotein complexes, including the small ribosomal subunit (Kim et al., 2014; Kuglstatter et al., 2002; Stern et al., 1989; Stone et al., 2007), and supports the role of r-proteins as built-in "assembly helpers."

Potential Involvement of Factors in Late Assembly and the Folding of the PTC

The notion that the formation of the PTC appears to be first of all an rRNA folding problem may also explain why ribosome assembly *in vivo* depends on the support of assembly factors (Davis and Williamson, 2017; Shajani et al., 2011). Even though many such factors are known, their precise mode of action is elusive in most cases, and crucial evidence for their role in assembly is based on gene deletion experiments (Kaczanowska and Rydén-Aulin, 2007; Shajani et al., 2011; Verstraeten et al., 2011). For example, the absence of the *E. coli* GTPases EngA and ObgE or the *Bacillus subtilis* GTPases RbgA, YphC (EngA homolog), and YsxC (EngB homolog) leads to the accumulation of ~45S precursors (Ni et al., 2016; Verstraeten et al., 2011). In all these precursors, the late assembly proteins uL16, bL27, bL28, bL33, bL35, and bL36 are absent or severely depleted.

Interestingly, intermediate resolution cryo-EM reconstructions of 50S intermediates derived from *ΔYphC* and *ΔYsxC* cells (Ni et al., 2016) appear similar to our reconstruction of state 1, and most of the subclasses that were obtained by Ni and colleagues are lacking density for the CP, L1 stalk, and stalk base. In addition, intermediate resolution cryo-EM maps of EngA and ObgE bound to 50S subunits are available (Feng et al., 2014; Zhang et al., 2014). Binding of EngA close to the E-site is only possible when bL33 and bL35 are absent (Zhang et al., 2014), a situation that is provided in states 1, 2, and 3. On the other hand, ObgE, which is known to act downstream of EngA (Karbstein, 2007), could bind to states 4 and 5 without obvious steric hindrance. Both EngA and ObgE insert domains into the PTC cleft (Feng et al., 2014; Zhang et al., 2014), indicating that both factors could target the non-native, alternative RNA structures within the PTC. Thus, it is tempting to speculate that EngA and ObgE act as assembly factors by remodeling the critical 23S rRNA region that will form the PTC.

A particular residue within the PTC region, U2552 of H92 (A-loop), is the target of the RNA methyltransferase RlmE (Caldas et al., 2000). Characteristically, *rlmE* deletion mutants harbor immature large subunits with pronounced structural flexibility affecting H89, 91, 92, and 71 and lack uL16, bL35, and bL36 when analyzed at low Mg^{2+} concentrations (Arai et al., 2015; Bügl et al., 2000). Moreover, a *ΔrpmJ* (bL36), *ΔrlmE* double mutant exhibits severe synthetic growth defects, indicating strong cooperativity between incorporation of bL36 and RlmE-mediated modification of U2552. Methylation of U2552, in turn, seems to be of critical importance to support a tripartite interaction between residues mU2552, C2556, and C1955 (Arai et al., 2015). This remarkable H-bond network establishes a crucial inter-domain contact between H71 in domain IV and H92 in domain V and is clearly absent, even in state 5. Concomitantly, density for bL36 is lacking, suggesting that bL36 may be involved in mediating the contact between H71 and H92. However, structural refinement of 50S rec^+ after step 2 incubation revealed persistent absence of bL36 but a natively structured PTC and a 50S-like overall structure (Figures S5F–S5H). This demonstrates that the maturation of the PTC is likely to be the key step in late 50S assembly, while the presence of the nonessential bL36 seems to be redundant.

The PTC is the ancient catalytic core of the ribosome (Polacek and Mankin, 2005) and, possibly as a consequence, free of r-proteins that could aid RNA folding. This absence of internal assembly helpers rationalizes that the maturation of the PTC is time consuming *in vitro* and requires temporary assistance *in vivo* provided by external assembly factors. Hence, the fact that the catalytic center of the 50S subunit resolves late *in vivo* (Arai et al., 2015; Jomaa et al., 2014; Li et al., 2013a; Ni et al., 2016) and last during *in vitro* assembly could represent a built-in quality-control mechanism to prevent untimely interaction with 30S subunits and participation in translation. Future studies are needed to address such concepts and further define the

relationship between the intrinsic assembly capacity of core ribosomal subunit components and the steering or modulation of this process *in vivo*.

STAR★METHODS

Detailed methods are provided in the online version of this paper and include the following:

- KEY RESOURCES TABLE
- CONTACT FOR REAGENT AND RESOURCE SHARING
- METHOD DETAILS
  - Isolation of 50S Subunits
  - 50S Total Reconstitution
  - Mass Spectrometry
  - Cryo-electron Microscopy and Data Processing
  - Model Building

SUPPLEMENTAL INFORMATION

Supplemental Information includes seven figures and two tables and can be found with this article online at https://doi.org/10.1016/j.molcel.2018.05.003.

ACKNOWLEDGMENTS

This work is dedicated to Knud H. Nierhaus, who sadly passed away during the preparation of the manuscript. We are grateful to Matthew L. Kraushar for critical review of the manuscript and fruitful discussions. This work was funded by the Human Frontier Science Program Organization (HFSP-Ref. RPG0008/2014) to K.H.N. and Deutsche Forschungsgemeinschaft grants FOR1805 and SFB740 to C.M.T.S. The authors acknowledge the North-German Supercomputing Alliance (HLRN) (beb 00007) for providing HPC resources that have contributed to the research results reported in this paper.

AUTHOR CONTRIBUTIONS

R.N. led the project; T.H. refined the data; R.N. and T.H. analyzed data, interpreted results, and prepared figures; B.Q. prepared the samples, performed biochemical experiments, analyzed data, and contributed figures; T.M. and J.B. applied sample, operated the electron microscope, and performed data acquisition; K.T.-T. performed q-MS experiments and evaluated the data; J.L. performed the movie correction and particle polishing; K.H.N. and C.M.T.S. conceived the project; C.M.T.S. supervised the study; and R.N., T.H., and C.M.T.S. wrote the manuscript.

DECLARATION OF INTERESTS

The authors declare no competing interests.

Received: August 8, 2017
Revised: February 27, 2018
Accepted: May 1, 2018
Published: June 7, 2018

REFERENCES

Adams, P.D., Afonine, P.V., Bunkóczi, G., Chen, V.B., Davis, I.W., Echols, N., Headd, J.J., Hung, L.W., Kapral, G.J., Grosse-Kunstleve, R.W., et al. (2010). PHENIX: a comprehensive Python-based system for macromolecular structure solution. Acta Crystallogr. D Biol. Crystallogr. *66*, 213–221.

Arai, T., Ishiguro, K., Kimura, S., Sakaguchi, Y., Suzuki, T., and Suzuki, T. (2015). Single methylation of 23S rRNA triggers late steps of 50S ribosomal subunit assembly. Proc. Natl. Acad. Sci. USA *112*, E4707–E4716.

Britton, R.A. (2009). Role of GTPases in bacterial ribosome assembly. Annu. Rev. Microbiol. *63*, 155–176.

Bügl, H., Fauman, E.B., Staker, B.L., Zheng, F., Kushner, S.R., Saper, M.A., Bardwell, J.C., and Jakob, U. (2000). RNA methylation under heat shock control. Mol. Cell *6*, 349–360.

Burakovsky, D.E., Sergiev, P.V., Steblyanko, M.A., Konevega, A.L., Bogdanov, A.A., and Dontsova, O.A. (2011). The structure of helix 89 of 23S rRNA is important for peptidyl transferase function of Escherichia coli ribosome. FEBS Lett. *585*, 3073–3078.

Caldas, T., Binet, E., Bouloc, P., Costa, A., Desgres, J., and Richarme, G. (2000). The FtsJ/RrmJ heat shock protein of Escherichia coli is a 23 S ribosomal RNA methyltransferase. J. Biol. Chem. *275*, 16414–16419.

Chen, J.Z., and Grigorieff, N. (2007). SIGNATURE: a single-particle selection system for molecular electron microscopy. J. Struct. Biol. *157*, 168–173.

Chen, S.S., and Williamson, J.R. (2013). Characterization of the ribosome biogenesis landscape in E. coli using quantitative mass spectrometry. J. Mol. Biol. *425*, 767–779.

Cox, J., Hein, M.Y., Luber, C.A., Paron, I., Nagaraj, N., and Mann, M. (2014). Accurate proteome-wide label-free quantification by delayed normalization and maximal peptide ratio extraction, termed MaxLFQ. Mol. Cell. Proteomics *13*, 2513–2526.

Davis, J.H., and Williamson, J.R. (2017). Structure and dynamics of bacterial ribosome biogenesis. Philos. Trans. R. Soc. Lond. B Biol. Sci. *372*, 372.

Davis, J.H., Tan, Y.Z., Carragher, B., Potter, C.S., Lyumkis, D., and Williamson, J.R. (2016). Modular assembly of the bacterial large ribosomal subunit. Cell *167*, 1610–1622.

Deutscher, M.P., Marlor, C.W., and Zaniewski, R. (1984). Ribonuclease T: new exoribonuclease possibly involved in end-turnover of tRNA. Proc. Natl. Acad. Sci. USA *81*, 4290–4293.

Dohme, F., and Nierhaus, K.H. (1976a). Role of 5S RNA in assembly and function of the 50S subunit from Escherichia coli. Proc. Natl. Acad. Sci. USA *73*, 2221–2225.

Dohme, F., and Nierhaus, K.H. (1976b). Total reconstitution and assembly of 50 S subunits from Escherichia coli Ribosomes in vitro. J. Mol. Biol. *107*, 585–599.

Dunkle, J.A., Wang, L., Feldman, M.B., Pulk, A., Chen, V.B., Kapral, G.J., Noeske, J., Richardson, J.S., Blanchard, S.C., and Cate, J.H. (2011). Structures of the bacterial ribosome in classical and hybrid states of tRNA binding. Science *332*, 981–984.

Eistetter, A.J., Butler, P.D., Traut, R.R., and Fanning, T.G. (1999). Characterization of Escherichia coli 50S ribosomal protein L31. FEMS Microbiol. Lett. *180*, 345–349.

Emsley, P., and Cowtan, K. (2004). Coot: model-building tools for molecular graphics. Acta Crystallogr. D Biol. Crystallogr. *60*, 2126–2132.

Feng, B., Mandava, C.S., Guo, Q., Wang, J., Cao, W., Li, N., Zhang, Y., Zhang, Y., Wang, Z., Wu, J., et al. (2014). Structural and functional insights into the mode of action of a universally conserved Obg GTPase. PLoS Biol. *12*, e1001866.

Franceschi, F.J., and Nierhaus, K.H. (1990). Ribosomal proteins L15 and L16 are mere late assembly proteins of the large ribosomal subunit. Analysis of an Escherichia coli mutant lacking L15. J. Biol. Chem. *265*, 16676–16682.

Frank, J., Radermacher, M., Penczek, P., Zhu, J., Li, Y., Ladjadj, M., and Leith, A. (1996). SPIDER and WEB: processing and visualization of images in 3D electron microscopy and related fields. J. Struct. Biol. *116*, 190–199.

Herold, M., and Nierhaus, K.H. (1987). Incorporation of six additional proteins to complete the assembly map of the 50 S subunit from Escherichia coli ribosomes. J. Biol. Chem. *262*, 8826–8833.

Jomaa, A., Jain, N., Davis, J.H., Williamson, J.R., Britton, R.A., and Ortega, J. (2014). Functional domains of the 50S subunit mature late in the assembly process. Nucleic Acids Res. *42*, 3419–3435.

Kaczanowska, M., and Rydén-Aulin, M. (2007). Ribosome biogenesis and the translation process in Escherichia coli. Microbiol. Mol. Biol. Rev. *71*, 477–494.

Karbstein, K. (2007). Role of GTPases in ribosome assembly. Biopolymers *87*, 1–11.

Kim, H., Abeysirigunawarden, S.C., Chen, K., Mayerle, M., Ragunathan, K., Luthey-Schulten, Z., Ha, T., and Woodson, S.A. (2014). Protein-guided RNA dynamics during early ribosome assembly. Nature *506*, 334–338.

Kucukelbir, A., Sigworth, F.J., and Tagare, H.D. (2014). Quantifying the local resolution of cryo-EM density maps. Nat. Methods *11*, 63–65.

Kuglstatter, A., Oubridge, C., and Nagai, K. (2002). Induced structural changes of 7SL RNA during the assembly of human signal recognition particle. Nat. Struct. Biol. *9*, 740–744.

Lancaster, L., Lambert, N.J., Maklan, E.J., Horan, L.H., and Noller, H.F. (2008). The sarcin-ricin loop of 23S rRNA is essential for assembly of the functional core of the 50S ribosomal subunit. RNA *14*, 1999–2012.

Lehmann, A., Niewienda, A., Jechow, K., Janek, K., and Enenkel, C. (2010). Ecm29 fulfils quality control functions in proteasome assembly. Mol. Cell *38*, 879–888.

Leidig, C., Thoms, M., Holdermann, I., Bradatsch, B., Berninghausen, O., Bange, G., Sinning, I., Hurt, E., and Beckmann, R. (2014). 60S ribosome biogenesis requires rotation of the 5S ribonucleoprotein particle. Nat. Commun. *5*, 3491.

Li, N., Chen, Y., Guo, Q., Zhang, Y., Yuan, Y., Ma, C., Deng, H., Lei, J., and Gao, N. (2013a). Cryo-EM structures of the late-stage assembly intermediates of the bacterial 50S ribosomal subunit. Nucleic Acids Res. *41*, 7073–7083.

Li, X., Mooney, P., Zheng, S., Booth, C.R., Braunfeld, M.B., Gubbens, S., Agard, D.A., and Cheng, Y. (2013b). Electron counting and beam-induced motion correction enable near-atomic-resolution single-particle cryo-EM. Nat. Methods *10*, 584–590.

Loerke, J., Giesebrecht, J., and Spahn, C.M. (2010). Multiparticle cryo-EM of ribosomes. Methods Enzymol. *483*, 161–177.

Mizushima, S., and Nomura, M. (1970). Assembly mapping of 30S ribosomal proteins from E. coli. Nature *226*, 1214.

Ni, X., Davis, J.H., Jain, N., Razi, A., Benlekbir, S., McArthur, A.G., Rubinstein, J.L., Britton, R.A., Williamson, J.R., and Ortega, J. (2016). YphC and YsxC GTPases assist the maturation of the central protuberance, GTPase associated region and functional core of the 50S ribosomal subunit. Nucleic Acids Res. *44*, 8442–8455.

Nierhaus, K.H. (1991). The assembly of prokaryotic ribosomes. Biochimie *73*, 739–755.

Nierhaus, K.H., and Dohme, F. (1974). Total reconstitution of functionally active 50S ribosomal subunits from Escherichia coli. Proc. Natl. Acad. Sci. USA *71*, 4713–4717.

Pettersen, E.F., Goddard, T.D., Huang, C.C., Couch, G.S., Greenblatt, D.M., Meng, E.C., and Ferrin, T.E. (2004). UCSF Chimera–a visualization system for exploratory research and analysis. J. Comput. Chem. *25*, 1605–1612.

Polacek, N., and Mankin, A.S. (2005). The ribosomal peptidyl transferase center: structure, function, evolution, inhibition. Crit. Rev. Biochem. Mol. Biol. *40*, 285–311.

Ratje, A.H., Loerke, J., Mikolajka, A., Brünner, M., Hildebrand, P.W., Starosta, A.L., Dönhöfer, A., Connell, S.R., Fucini, P., Mielke, T., et al. (2010). Head swivel on the ribosome facilitates translocation by means of intra-subunit tRNA hybrid sites. Nature *468*, 713–716.

Röhl, R., and Nierhaus, K.H. (1982). Assembly map of the large subunit (50S) of Escherichia coli ribosomes. Proc. Natl. Acad. Sci. USA *79*, 729–733.

Rohou, A., and Grigorieff, N. (2015). CTFFIND4: fast and accurate defocus estimation from electron micrographs. J. Struct. Biol. *192*, 216–221.

Selmer, M., Dunham, C.M., Murphy, F.V., 4th, Weixlbaumer, A., Petry, S., Kelley, A.C., Weir, J.R., and Ramakrishnan, V. (2006). Structure of the 70S ribosome complexed with mRNA and tRNA. Science *313*, 1935–1942.

Shajani, Z., Sykes, M.T., and Williamson, J.R. (2011). Assembly of bacterial ribosomes. Annu. Rev. Biochem. *80*, 501–526.

Sieber, G., and Nierhaus, K.H. (1978). Kinetic and thermodynamic parameters of the assembly in vitro of the large subunit from Escherichia coli ribosomes. Biochemistry *17*, 3505–3511.

Siibak, T., Peil, L., Xiong, L., Mankin, A., Remme, J., and Tenson, T. (2009). Erythromycin- and chloramphenicol-induced ribosomal assembly defects are secondary effects of protein synthesis inhibition. Antimicrob. Agents Chemother. *53*, 563–571.

Spillmann, S., Dohme, F., and Nierhaus, K.H. (1977). Assembly in vitro of the 50 S subunit from Escherichia coli ribosomes: proteins essential for the first heat-dependent conformational change. J. Mol. Biol. *115*, 513–523.

Sprink, T., Ramrath, D.J., Yamamoto, H., Yamamoto, K., Loerke, J., Ismer, J., Hildebrand, P.W., Scheerer, P., Bürger, J., Mielke, T., and Spahn, C.M. (2016). Structures of ribosome-bound initiation factor 2 reveal the mechanism of subunit association. Sci. Adv. *2*, e1501502.

Stern, S., Powers, T., Changchien, L.M., and Noller, H.F. (1989). RNA-protein interactions in 30S ribosomal subunits: folding and function of 16S rRNA. Science *244*, 783–790.

Stone, M.D., Mihalusova, M., O'connor, C.M., Prathapam, R., Collins, K., and Zhuang, X. (2007). Stepwise protein-mediated RNA folding directs assembly of telomerase ribonucleoprotein. Nature *446*, 458–461.

Suloway, C., Pulokas, J., Fellmann, D., Cheng, A., Guerra, F., Quispe, J., Stagg, S., Potter, C.S., and Carragher, B. (2005). Automated molecular microscopy: the new Leginon system. J. Struct. Biol. *151*, 41–60.

Sykes, M.T., Shajani, Z., Sperling, E., Beck, A.H., and Williamson, J.R. (2010). Quantitative proteomic analysis of ribosome assembly and turnover in vivo. J. Mol. Biol. *403*, 331–345.

Traub, P., and Nomura, M. (1968). Structure and function of E. coli ribosomes. V. Reconstitution of functionally active 30S ribosomal particles from RNA and proteins. Proc. Natl. Acad. Sci. USA *59*, 777–784.

Verstraeten, N., Fauvart, M., Versées, W., and Michiels, J. (2011). The universally conserved prokaryotic GTPases. Microbiol. Mol. Biol. Rev. *75*, 507–542.

Wu, S., Tutuncuoglu, B., Yan, K., Brown, H., Zhang, Y., Tan, D., Gamalinda, M., Yuan, Y., Li, Z., Jakovljevic, J., et al. (2016). Diverse roles of assembly factors revealed by structures of late nuclear pre-60S ribosomes. Nature *534*, 133–137.

Yamamoto, H., Wittek, D., Gupta, R., Qin, B., Ueda, T., Krause, R., Yamamoto, K., Albrecht, R., Pech, M., and Nierhaus, K.H. (2016). 70S-scanning initiation is a novel and frequent initiation mode of ribosomal translation in bacteria. Proc. Natl. Acad. Sci. U.S.A *113*, e1180–e1189.

Youngman, E.M., Brunelle, J.L., Kochaniak, A.B., and Green, R. (2004). The active site of the ribosome is composed of two layers of conserved nucleotides with distinct roles in peptide bond formation and peptide release. Cell *117*, 589–599.

Zhang, X., Yan, K., Zhang, Y., Li, N., Ma, C., Li, Z., Zhang, Y., Feng, B., Liu, J., Sun, Y., et al. (2014). Structural insights into the function of a unique tandem GTPase EngA in bacterial ribosome assembly. Nucleic Acids Res. *42*, 13430–13439.

Zheng, S.Q., Palovcak, E., Armache, J.P., Verba, K.A., Cheng, Y., and Agard, D.A. (2017). MotionCor2: anisotropic correction of beam-induced motion for improved cryo-electron microscopy. Nat. Methods *14*, 331–332.

STAR★METHODS

KEY RESOURCES TABLE

REAGENT or RESOURCE	SOURCE	IDENTIFIER
Bacterial and Virus Strains		
CAN20-12E (RNase $I^-II^-D^-BN^-$)	Deutscher et al., 1984	N/A
Deposited Data		
Quantitative mass spectrometry data tables	This study	https://dx.doi.org/10.17632/7392gfb2ps.1
Cryo-EM density map: State_1	This study	EMD: 4382
Cryo-EM density map: State_2	This study	EMD: 4381
Cryo-EM density map: State_3	This study	EMD: 4380
Cryo-EM density map: State_4	This study	EMD: 4379
Cryo-EM density map: State_5	This study	EMD: 4378
Cryo-EM density map: 50S rec^+	This study	EMD: 4383
Atomic model: State_1	This study	PDB: 6GC7
Atomic model: State_2	This study	PDB: 6GC6
Atomic model: State_3	This study	PDB: 6GC4
Atomic model: State_4	This study	PDB: 6GC0
Atomic model: State_5	This study	PDB: 6GBZ
Atomic model: State_50S rec^+	This study	PDB: 6GC8
Software and Algorithms		
Leginon	Suloway et al., 2005	http://emg.nysbc.org/redmine/projects/leginon/wiki/Leginon_Homepage
MotionCorr	Li et al., 2013b	http://cryoem.ucsf.edu/software/driftcorr.html
CTFFIND4	Rohou and Grigorieff, 2015	http://grigoriefflab.janelia.org/ctffind4
SIGNATURE	Chen and Grigorieff, 2007	http://grigoriefflab.janelia.org/signature
SPIDER	Frank et al., 1996	https://spider.wadsworth.org/
ResMap	Kucukelbir et al., 2014	http://resmap.sourceforge.net/
MotionCor2	Zheng et al., 2017	http://msg.ucsf.edu/em/software/motioncor2.html
Chimera	Pettersen et al., 2004	https://www.cgl.ucsf.edu/chimera/
Coot	Emsley and Cowtan, 2004	http://www2.mrc-lmb.cam.ac.uk/Personal/pemsley/coot/
MDfit	Ratje et al., 2010	http://sanbonmatsu.org/gmx-4.5.5-mdfit.tar.gz
PHENIX	Adams et al., 2010	https://www.phenix-online.org/
Mascot v.2.6.1	Matrix Science	http://www.matrixscience.com
MaxQuant v.1.6.0.81	Cox et al., 2014	http://www.coxdocs.org/doku.php?id=maxquant:start
Other		
E. coli 23S rRNA secondary structure map	Noller laboratory	http://rna.ucsc.edu/rnacenter/images/figs/ecoli_23s.jpg

CONTACT FOR REAGENT AND RESOURCE SHARING

Further information and requests for reagents should be directed to Lead Contact Dr. Christian M. T. Spahn (christian.spahn@charite.de).

METHOD DETAILS

Isolation of 50S Subunits

50S subunits were isolated from mid-exponential cultures of *E. coli* CAN20-12E (Deutscher et al., 1984) according to a protocol described previously (Dohme and Nierhaus, 1976b).

50S Total Reconstitution

50S Reconstitution Assay Step 1

The assay was performed according to Dohme and Nierhaus (1976b) with the modifications described in Nierhaus (1991). In step 1 of the 50S reconstitution 24 equivalent units of TP50 (total protein of the 50S subunit) and 30 A_{260} 23S rRNA + 5S rRNA were mixed and incubated for 30 min at 44°C in Rec 4 buffer (20 mM HEPES/KOH pH7.6 on ice, 400 mM NH_4Ac, 4 mM $Mg(Ac)_2$, 0.2 mM EDTA, 5 mM 2-mercapto-ethanol).

50S Reconstitution Assay Step 2

Material from step 1, or purified 48S aliquots were adjusted to 20 mM $Mg(Ac)_2$ concentration and incubated (90 min at 50°C) in the absence or presence of TP50. Total reconstitution of 50S subunits (50S rec.) was done as described earlier (Dohme and Nierhaus, 1976b). In brief: Two samples (containing TP50, 23S rRNA and 5S rRNA in Rec 4 buffer) were subjected to consecutive step 1 and 2 incubations.

Preparation of Non-purified Step 1 Precursors

A step 1 reaction was performed as described above, and the reaction products were diluted to a particle concentration of ~3 A_{260}/ml, with a final NH_4Ac concentration of 220 mM and subjected to cryo-EM analysis.

Preparation of Purified 48S or 41S Precursors

The products of two independent step 1 reactions were subjected to preparative (10%–30%) sucrose density gradient ultra-centrifugations in an SW32 rotor at 25,000 rpm and 4°C for 21 hr. Fractions containing 48S particles, or 41S particles, respectively, were pooled. The precursors were independently pelleted (45Ti rotor, 35,000 rpm for 20 hr), resuspended in Rec 4 buffer and aliquoted. Material from one aliquot was diluted to a particle concentration of ~3 A_{260}/ml, with a final NH_4Ac concentration of 220 mM and subjected to cryo-EM analysis. Another aliquot was used for an analytical (10%–30%) sucrose density gradient ultra-centrifugation (SW40 rotor, 26,000 rpm for 22 hr).

Preparation of 50S rec^- and 50S rec^+

A step 1 reaction was performed as described above. The reaction products were subjected to a preparative (10%–30%) sucrose density gradient ultra-centrifugation in an SW32 rotor at 25,000 rpm and 4°C for 21 hr. Fractions containing 48S particles were pooled. The pooled material was pelleted (45Ti rotor, 35,000 rpm for 20 hr), resuspended in Rec 4 buffer and adjusted to the buffer conditions of the step two reaction. The step 2 reaction was performed for 90 min at 50°C in absence or presence of L-proteins, producing 50S rec^-, or 50S rec^+, respectively. 50S rec^+ material was diluted to a particle concentration of ~3 A_{260}/ml, with a final NH_4Ac concentration of 220 mM and subjected to cryo-EM analysis.

Time Course Reconstitution Assay Step 1

TP50 and rRNA for a step 1 reaction were mixed on ice as described above. A first aliquot was taken instantaneously (0 min). The reaction tube was transferred to a preheated thermo-block (44°C) and further aliquots were taken after 2, 5, 10, 20 and 30 min of incubation. Material taken at the individual time points was subjected to analytical (10%–30%) sucrose density gradient ultra-centrifugation (SW55 rotor, 32,000 rpm for 2 hr).

Time Course Reconstitution Assay Step 2

After standard step 1 reaction (30 min at 44°C), conditions were adjusted to step 2 reaction (20 mM $Mg(Ac)_2$, 50°C). After 0, 15, 30, 60 and 90 min of incubation aliquots were taken and subjected to analytical (10%–30%) sucrose density gradient ultra-centrifugation (SW55 rotor, 32,000 rpm for 2,5 hr).

Poly (U)-Dependent Poly (Phe) Assay

6 pmol isolated native 50S subunits (50S), reconstituted 50S subunits (50S rec.), purified 48S precursors (48S), and 48S precursors that had been converted into 50S particles by step 2 incubation in the absence (48S -) or presence (48S +) of TP50 were subjected to assays as described (Yamamoto et al., 2016), mixed with 12 pmol 30S subunits and incubated in assay buffer (20 mM HEPES/KOH pH7.6 on ice, 150 mM NH_4 Ac, 6 mM $Mg(Ac)_2$, 0.05 mM EDTA, 4 mM 2-mercaptoethanol, 0.05 mM spermine, 2 mM spermidine, 3 mM ATP, 1.5 mM GTP, 83 μM acetyl-Phe and 0.83 μCi/ml ^{14}C labeled acetyl-Phe, 0.83 mg/ml polyU, 340 mg/ml tRNA and S100 extract) for 60 min at 37°C. Then, 30 μl BSA (1% stock solution) and 2ml TCA (10%) were added. Samples were briefly vortexed, incubated for 15 min at 90°C and 5 min on ice. Precipitated proteins were immobilized on glass filters, washed two times with 5% TCA and once with diethylether/ethanol (1:1). The filters were incubated in scintillation liquid and the amount of incorporated ^{14}C Phe was determined using a scintillation counter. The assay was done in duplicates and mean values were calculated.

Mass Spectrometry

Sample Preparation

Amounts of TP50, native 50S subunits and isolated 48S material corresponding to app. 10 μg total protein, were mixed with 4X LDS sample buffer (Thermo Fisher Scientific) and subjected to SDS-PAGE analysis using 4%–12% NuPAGE gradient gels (Thermo Fisher Scientific). The protein content was separated for 10 min at 150 mV. Proteins were stained for 1 hr with SimplyBlue SafeStain solution (Thermo Fisher Scientific). After 1 hr of destaining in deionized H_2O, gel regions containing the separated proteins of TP50, 50S and 48S material, respectively, were split into thirds. Each third was subsequently reduced to small pieces with 1-2 mm edge length. For identification and relative quantification of the r-proteins, gel pieces with the contained proteins were subjected to tryptic digest, as described previously (Lehmann et al., 2010).

LC-MS Analysis

The LC-MSMS analyses of tryptic peptides have been performed as follows. Samples were concentrated for 2 min on a trap column (PepMap C18, 5 mm x 300 μm x 5 μm, 100Å, Thermo Fisher Scientific) with 2:98 (v/v) acetonitrile/water containing 0.1% (v/v) trifluoroacetic acid at a flow rate of 30 μl/min and then analyzed by nanoscale LC-MS/MS measurements using a Q Exactive Plus mass spectrometer coupled with an Ultimate 3000 RSLCnano (Thermo Fisher Scientific). The system comprised a 75 μm i.d. × 250 mm nano LC column (Acclaim PepMap C18, 2 μm; 100 Å; Thermo Fisher Scientific). The mobile phase (A) consisted of 0.1% (v/v) formic acid (FA) in water, and (B) of 80:20 (v/v) acetonitrile/water containing 0.1% (v/v) FA. Elution took place using a gradient 3%–38% B in 95 min with a flow rate of 300 nl/min. Full MS spectra (m/z 200–1,600) have been acquired at a resolution of 70,000 (FWHM) followed by a data-dependent MS/MS fragmentation of the top6 precursor ions (dissociation method HCD, resolution 17,500, 1+ charge state excluded, isolation window of 1.6 m/z, NCE of 27%, dd 60 s). Maximum ion injection time has been set to 100 ms and for MS and to 160 ms for MS/MS scans. Background ions at m/z 391.2843 and 445.1200 acted as lock masses.

Bioinformatic Processing

Proteins were identified by Mascot software version 2.6.1. (Matrix Science, London, UK) using the following search parameter set. database: SwissProt, taxonomy: *E. coli*, enzyme: trypsin/P with two missed cleavage, static modification: carbamidomethylation (C), variable modifications: protein N-acetylation and oxidation (M), mass tolerances for MS and MSMS: 5 ppm and 0.02 Da, and a calculated peptide FDR 1%.

Relative label free quantification of the r-proteins was performed with MaxQuant (version 1.6.0.1; Cox et al., 2014) and default Andromeda LFQ parameters. Spectra were matched to an *E. coli* database (23,031 reviewed entries, downloaded from uniprot.org), a contaminant database, and a decoy database. Search parameters were used as described above. In addition, protein identifications were calculated with FDR = 1% and proteins with one razor peptide per protein were included for subsequent analyses.

Cryo-electron Microscopy and Data Processing

3.6 μl of purified 48S precursors, non-purified precursors after 30 min step 1 incubation, and 50S subunits formed after 90 min step 2 incubation in the presence of TP50 (50S rec$^+$), respectively, were spotted on glow-discharged holey carbon grids (Quantifoil Micro Tools GmbH) and cryo plunged in liquid ethane after blotting using a Vitrobot device (FEI). Imaging was done with a FEI Tecnai G2 Polara at 300 keV, equipped with a K2 Summit (Gatan) running in movie mode at a nominal magnification of 80,645x. The corresponding pixel size was 0.62 Å on the object scale. 25 movie frames were collected per image with a total exposure time of 5 s, yielding an electron dose of 25 $e^-/Å^2$. Automated image collection was done with Leginon (Suloway et al., 2005) at a defocus range between 0.5 and 5 μm (Table S2). Movie frames were corrected for drift using MotionCorr (Li et al., 2013b), defocus estimation was done with CTFFIND4 (Rohou and Grigorieff, 2015). For the 48S precursor sample, 1684 micrographs were subjected to semi-automated particle picking with SIGNATURE (Chen and Grigorieff, 2007) using projections of a 50S ribosomal subunit as reference. A total of 154462 particle images was used for multiparticle refinement (Loerke et al., 2010) with SPIDER (Frank et al., 1996) (Figure S2). Again, a 50S ribosome was used as initial reference for particle alignment and subsequent classifications. Importantly, no mature 50S subunit was obtained within the sorting. Four meaningful ribosomal structures were identified, isolated, and refined individually. FSC resolution measurements were performed semi-independently, local resolutions were determined with ResMap (Kucukelbir et al., 2014) using half-maps.

In the case of the non-purified step 1 precursors, 4311 micrographs were refined independently in the same manner, with the exception that MotionCor2 (Zheng et al., 2017) was applied for movie correction and dose weighting (5x5 patches). Multi-particle refinement revealed altered occupancies of the resulting populations, namely a shift toward the earlier states. This allowed the separation of the least mature state into two sub-populations, revealing an additional even less mature state compared with the 48S precursor sample.

For the 50S rec$^+$ sample 1,144 micrographs were collected as previously. Of the initially identified 116,500 particle images, 94% were assigned to a mature 50S subunit. Importantly, despite using the state 5 (purified 48S peak sample) structure as initial reference during refinement, no meaningful immature ribosomal structure was found. Due to a strong orientation bias, random particle images from the over-represented views were removed, reducing the final dataset to a number of 60906 images, yielding a resolution of 3.78 Å.

Model Building

Atomic models were generated based on the crystal structure of the *E.coli* ribosome (PDB: 3R8S; Dunkle et al., 2011) in three steps. First, rigid body fitting and manual truncation of unstructured regions was done with Chimera (Pettersen et al., 2004) and Coot (Emsley and Cowtan, 2004). Next, flexible fitting of the initial models was achieved by MDfit (Ratje et al., 2010) into low-resolution cryo-EM structures of our maps to avoid over-fitting into high-resolution features and to maintain secondary structure integrity. Alternative RNA structures were tentatively modeled manually in Coot. Initially, all models were real-space refined with PHENIX (Adams et al., 2010) as described previously (Sprink et al., 2016), using individually determined weight factors to avoid over-fitting.